Fluorescence quenching by photoinduced electron transfer in the Zn[superscript 2+] sensor Zinpyr-1: a computational investigation

Citation: Kowalczyk, Tim, Ziliang Lin, and Troy Van Voorhis. "Fluorescence Quenching by Photoinduced Electron Transfer in the Zn[superscript 2+] Sensor Zinpyr-1: A Computational Investigation." The Journal of Physical Chemistry A 114.38 (2010): 10427–10434.

As Published: http://dx.doi.org/10.1021/jp103153a

Publisher: American Chemical Society

Persistent URL: http://hdl.handle.net/1721.1/69659

Version: Author's final manuscript: final author's manuscript post peer review, without publisher's formatting or copy editing

Fluorescence quenching by photoinduced electron transfer in the Zn^{2+} sensor Zinpyr-1: a computational investigation

Tim Kowalczyk,[†] Ziliang Lin,[†,‡] and Troy Van Voorhis[*,†]

Department of Chemistry, Massachusetts Institute of Technology, Cambridge MA 02139

E-mail: tvan@mit.edu

[*]To whom correspondence should be addressed
[†]Department of Chemistry, Massachusetts Institute of Technology, Cambridge MA 02139
[‡]Present address: Department of Applied Physics, Stanford University, Stanford, CA 94305

Abstract

We report a detailed study of luminescence switching in the fluorescent zinc sensor Zinpyr-1 by density functional methods. A two-pronged approach employing both time-dependent density functional theory (TDDFT) and constrained density functional theory (CDFT) is used to characterize low-lying electronically excited states of the sensor. The calculations indicate that fluorescence activation in the sensor is governed by a photoinduced electron transfer mechanism in which the energy level ordering of the excited states is altered by binding Zn^{2+}. While the sensor is capable of binding two Zn^{2+} cations, a single Zn^{2+} ion appears to be sufficient to activate moderate fluorescence in aqueous solution at physiological pH. We show that it is reasonable to consider the tertiary amine as the effective electron donor in this system, although the pyridyl nitrogens each contribute some density to the xanthone ring. The calculations illustrate an important design principle: because protonation equilibria at receptor sites can play a determining role in the sensor's fluorescence response, receptor sites with a pK_a near the pH of the sample are to be disfavored if a sensor governed by a simple PET fluorescence quenching model is desired.

Keywords: charge transfer state; zinc; ZP1; constrained density functional theory; time-dependent density functional theory

Introduction

Photoinduced electron transfer (PET)[1,2] is the widely accepted mechanism for the behavior of a class of "turn-on" fluorescent chemosensors which fluoresce only in the presence of targeted analytes. These sensors are electron donor-acceptor systems in which the initial photoexcitation is localized on the acceptor (Figure 1a). In the absence of analyte, the HOMO of the donor lies higher in energy than that of the acceptor and can transfer an electron to the acceptor's HOMO. The electron transfer process competes favorably with radiative decay to the ground state, substantially diminishing the fluorescence quantum yield.[3] Binding of the sensor to its particular analyte lowers the donor HOMO below that of the acceptor HOMO, preventing electron transfer and favoring fluorescence. One may also consider PET from the perspective of electronic states (Figure 1b) instead of molecular orbitals. In this picture, the bare sensor possesses a charge-transfer (CT) excited state which lies energetically beneath the lowest optically active excited state and provides a nonradiative relaxation pathway for the photoexcited sensor. When the sensor binds its analyte, the CT state is shifted above the optically active state and can no longer quench the fluorescence.

PET and other luminescence switching mechanisms have been harnessed in the design of a variety of chemical sensors.[4,5] Desirable properties of the sensors, such as selectivity for the analyte and intensity of the fluorescence activation, can be tuned by the addition of functional groups which modify the sensor's electronic structure. The systematic optimization of fluorescence-based chemosensors is an active area of research.[4,6] The present study is motivated by the conviction that rational sensor design can benefit from computational insight into the photophysics of these sensors, especially as a predictive tool for features (such as the energetics of the CT state) that are difficult to probe experimentally.

In this article we describe a computational investigation of the photophysics of luminescence switching in the zinc-sensing fluorophore Zinpyr-1 (ZP1, Figure 2).[7,8] While PET is a likely mechanism for fluorescence quenching in ZP1, there are several alternatives[4,9] worth consideration.

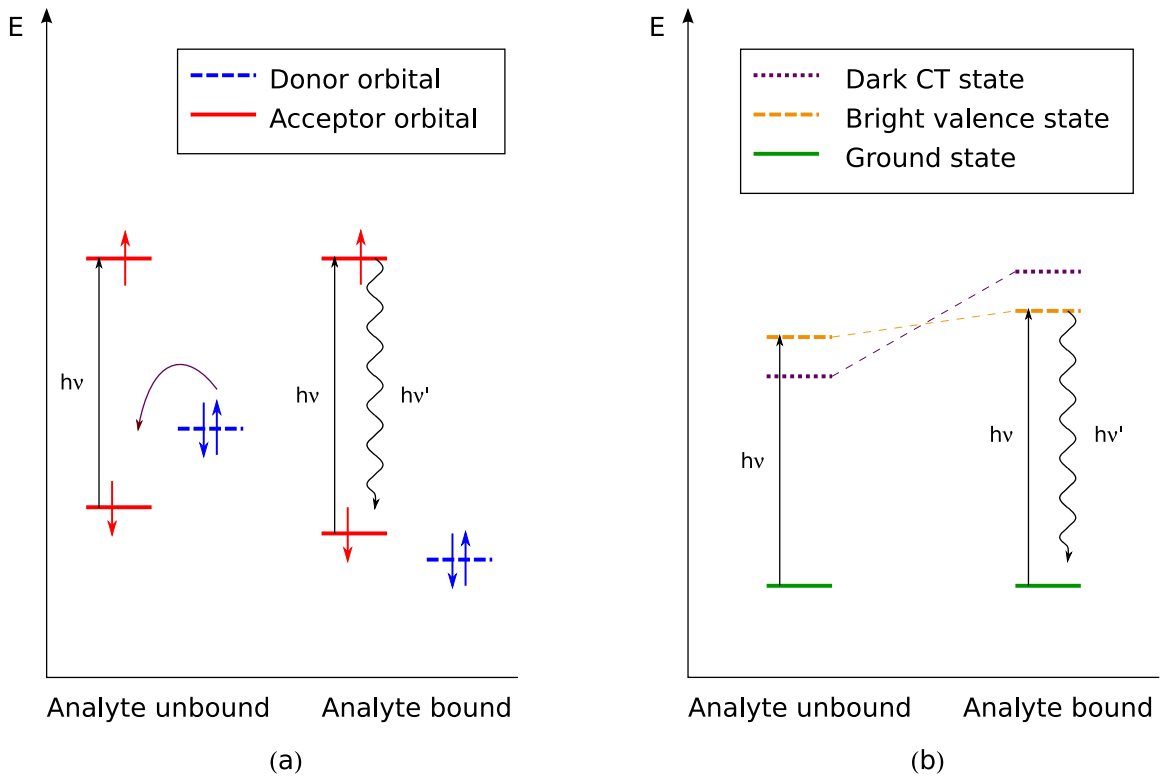

Figure 1: Energy level diagrams illustrating PET from (a) the frontier molecular orbital perspective and from (b) the electronic states perspective.

Among these, internal charge transfer,[10] excimer formation,[11] and resonance energy transfer[12] are all employed in sensor design, but these mechanisms are limited to molecular architectures[9] to which ZP1 does not conform. Proton-coupled electron transfer (PCET)[13] has been reported in some chemical sensors[14] and is a viable alternative to simple PET.

It has become somewhat routine for researchers in sensor design and synthesis to use time-dependent density functional theory (TDDFT) to calculate electronic spectra and assess whether the qualitative picture of PET holds for their sensors.[15–17] Petsalakis and coworkers report a series of studies[18,19] on pyrene-based fluorophores that led to a rule for predicting the strength of a PET process in terms of donor and acceptor orbital energies. Wang, Dyer and coworkers have illustrated the value of computation in sensor design by predicting the photophysical properties of a Zn^{2+} PET sensor and then assessing their predictions by synthesis and characterization of the sensor.[20] However, the reliance of previous computational studies on TDDFT methods is troublesome because TDDFT has a well-documented tendency to underestimate the energy of CT excited states.[21]

To address concerns about the reliability of CT excited states obtained from TDDFT, in this study we supplement conventional TDDFT calculations with a constrained DFT (CDFT) approach,[22] which enables an explicit construction of the diabatic states involved in electron transfer.[23] The CT excitation energy is given by the energy difference between these diabatic states. CDFT provides an alternative to TDDFT for the characterization of CT excited states. Together, the two methods allow for critical evaluation of the computations, as they approach the problem of CT excited states from different perspectives.

After a review of the salient chemical and photophysical properties of ZP1 obtained from previous experiments, we describe the details of our computational approach. We report TDDFT vertical excitation energies of ZP1 with traditional hybrid and long-range corrected (LRC) functionals and show that these computations are unable to clearly resolve the ordering of the low-lying

excited states. CT excitation energies deduced from CDFT calculations are then compared to valence excitation energies from TDDFT. Together, the two methods are shown to support the PET fluorescence quenching hypothesis. Finally we assess the merits and shortcomings of our approach and discuss some future directions for this investigation.

The Zn^{2+} chemosensor ZP1

Several examples of both one- and two-arm fluorescein-based zinc sensors have emerged since ZP1 was first characterized,[6] featuring improvements such as diminished background fluorescence of the metal-free chromophore,[24–26] reversible Zn^{2+} binding for monitoring zinc over time,[27,28] and ratiometric sensing for quantifying the concentration of Zn^{2+} in solution.[29] We have chosen to focus our modeling efforts on ZP1 because of the volume of experimental data available for this sensor and because of its established role as a template for future fluorescein-based zinc sensor design.[6]

ZP1 and several of its derivatives are effective probes of Zn^{2+} in biological settings and have made possible a number of important neurological and immunological studies on the bioactivity of zinc.[30,31] The sensor consists of a pair of di(2-picolyl)amine (DPA) arms covalently bonded to a 2′,7′-dichlorofluorescein (DCF) body at the 4′ and 5′ positions of the DCF ring (Figure 2). DPA is known to selectively bind Zn^{2+} over other dications encountered in physiological settings,[32] notably Ca^{2+} and Mg^{2+}. ZP1 can bind Zn^{2+} in either of two pockets formed by the chelating nitrogens of DPA and a carbonyl oxygen on the xanthone ring. We will denote ZP1 structures binding Zn^{2+} by Zn-ZP1 or Zn_2-ZP1, according to the number of Zn^{2+} ions bound.

In the absence of Zn^{2+} and at physiological pH, the absorption spectrum of ZP1 exhibits a maximum at $\lambda = 515$ nm, and the molecule fluoresces with a modest quantum yield $\Phi = 0.17$.[8] In saturated Zn^{2+} solution, the maximum absorption wavelength is blueshifted to 507 nm and the quantum yield increases to $\Phi = 0.87$. This enhancement of the fluorescence is quite selective for

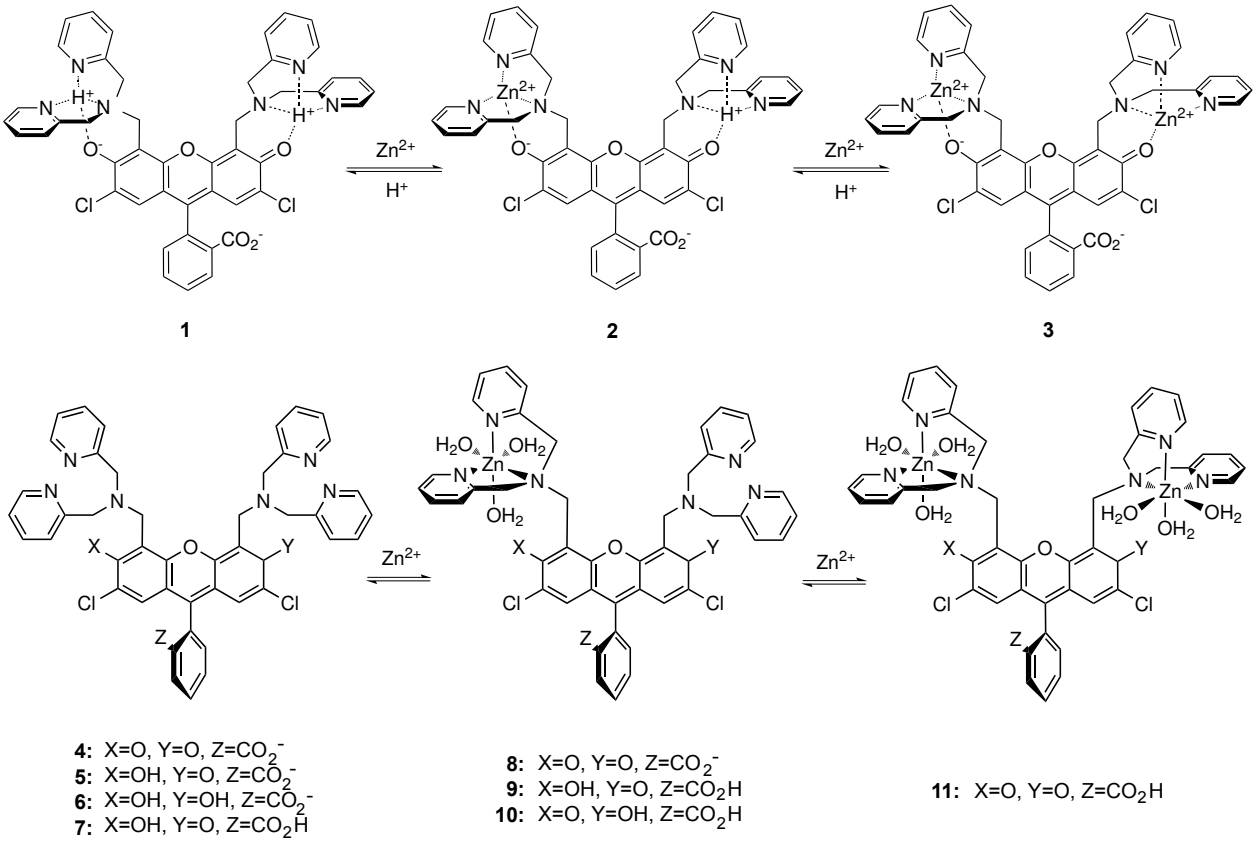

Figure 2: Top: schematic of Zn^{2+} binding to ZP1 in aqueous solution, with formal charges as indicated. Bottom: ZP1 structures employed in this study, including explicit coordination of water to Zn.

Zn^{2+}; only its d^{10} congener Cd^{2+} is known to induce a comparable fluorescence activation. This behavior is consistent with a PET mechanism in which the lowering of the donor HOMO is more pronounced upon binding to a filled *d* shell metal dication than to a dication with an unfilled *d* shell.[5]

A variety of protonation states are available to ZP1: four pyridyl nitrogens and the pair of ion-binding pockets are accessible for protonation, as well as the DCF carboxylate group. Accordingly, the fluorescence emission spectrum of ZP1 exhibits a complicated pH dependence, which has recently been explored in detail by potentiometric titration studies.[8] At neutral pH, one of the two binding pockets is protonated. Protonation of the second binding pocket corresponds to a pK_a of 6.96, indicating a mixture of occupied and free binding pockets at physiological pH. In aqueous Zn^{2+} solution, experimental evidence indicates significant fluorescence enhancement for ZP1 structures in which both coordination sites are occupied, relative to structures with at least one empty site.[8]

Computational Details

For each metal-coordination and protonation state of ZP1 under study, the ground state geometry was optimized using Kohn-Sham DFT with the B3LYP functional[33,34] as implemented in TURBOMOLE.[35] An SV(P) basis set[36] was employed for main group atoms, and a Stuttgart-Köln ECP was used for zinc.[37] The optimizations were performed in aqueous solution using the COSMO solvation model.[38] To account for direct coordination of the solvent to the metal, three explicit water molecules were ligated to Zn, resulting in an overall octahedral coordination.

Gas-phase TDDFT vertical excitation energies were evaluated with the B3LYP functional and SV(P) basis set, and solvation effects were studied with COSMO. Because conventional hybrid density functionals have a systematic tendency to underestimate CT excited state energies,[21] the recently developed long-range corrected LRC-PBE and LRC-PBE0 functionals of Herbert and

coworkers[39] were also employed for gas-phase TDDFT calculations in Q-CHEM.[40] In these functionals, full Hartree-Fock exchange is invoked for long-range interactions, while the generalized gradient (for PBE) or hybrid (for PBE0) exchange of the original functional is retained at short distances. An analytically smoothed cut-off between short- and long-ranged interactions is controlled by a range separation parameter ω. Attachment-detachment densities[41] of relevant electronic transitions were computed within the Tamm-Dancoff approximation.[42] The correlation-consistent cc-pVDZ and aug-cc-pVDZ basis sets[43] were used to gauge the adequacy of the smaller SV(P) basis for our TDDFT calculations.

Further characterization of the CT states was carried out using CDFT with the B3LYP functional and SV(P) basis set. In this method, the Kohn-Sham equations of DFT are solved in the presence of an auxiliary potential which constrains the net charge on user-defined donor and acceptor regions of the molecule to specific values. For example, the CT state of a neutral donor-acceptor molecule is defined by constraining the net charge on the donor to $+1$ and the net charge on the acceptor to -1. This approach yields the energies of the diabatic neutral and CT electronic states by ground state methods, providing an alternative to TDDFT for calculating the energy of CT excited states. Ground state molecular analysis techniques such as atomic population analysis[44] are also available for constrained states in CDFT. All reported TDDFT and CDFT excitation energies are vertical excitation energies.

Some additional care must be taken to correctly capture solvent stabilization of the CT state within the CDFT approach. The reorganization of solvent nuclear degrees of freedom to accommodate a modified charge distribution is a slow process relative to polarization of the solvent electron density.[45,46] Upon vertical excitation from the ground state, the CT state experiences nonequilibrium solvation in which the solvent electron density is equilibrated with respect to the density of the solute CT state but the solvent nuclear configuration is equilibrated with respect to the ground state density of the solute. To account for nonequilibrium solvation of the CT state, we employ a modified Onsager self-consistent reaction field (SCRF) model[47] in which the slow and

fast components of the polarization response are separated according to the Pekar partition.[48,49] We emphasize that this correction scheme only applies to vertical excitation energies, in which the solute nuclear configuration has not yet relaxed in response to the CT density. A solute radius $a_0 = 10$Å was chosen to ensure full electrostatic interaction between the solute density and the dielectric continuum while still encapsulating the solute density almost entirely within the cavity. The value $\varepsilon = 80$ was used for the static dielectric constant of water, and the fast dielectric constant was computed as the square of the index of refraction of water, $\varepsilon_\infty = 1.77$.

Results and Discussion

TDDFT with a conventional hybrid functional

Based on our understanding of the chemistry of ZP1 at neutral pH,[8] we expect the anion and neutral ZP1 structures **5** and **6** in Figure 2, which each have at least one deprotonated receptor site, to be important in biological applications. However, as noted by Baik and coworkers,[17] geometry optimizations on fluorescein-based sensors tend to converge to the nonfluorescent lactone isomer when the carboxylate is left deprotonated. In lieu of their constrained optimization approach, we attempted geometry optimizations for the carboxylate structures with the COSMO solvation model, rejecting structures which formed the lactone during this procedure.

Optimization of structures **4** and **5** did not result in lactone formation, so we proceeded to evaluate their vertical excitation spectra with TD-B3LYP/SV(P) in the gas phase and with COSMO. The doubly-protonated structure **6** relaxed to the lactone isomer even with COSMO solvation, so we included an explicit water molecule which acts as a hydrogen bond donor to discourage ring closure. This procedure resulted in a ring-opened optimized structure for **6**.

Gas-phase TDDFT calculations on **4** through **6** at the B3LYP/SV(P) level yielded several spurious low-lying CT excited states, as identified by their absence upon inclusion of solvation effects.

These spurious states are unsuitable for comparison with gas-phase excited states from other approaches. We therefore protonated the carboxylate group to obtain structure **7**, which is not expected to exist in aqueous solution, but which proved to be a useful benchmark for comparison to LRC-TDDFT and CDFT excited states, as its gas-phase excitation spectrum was not contaminated with low-lying CT states.

Although **7** is not expected to fluoresce,[50] experimental evidence[51] indicates that the lack of fluorescence in neutral fluorescein and its derivatives is due to fast conversion to the anion rather than to significant differences in the absorption spectra of the neutral and anionic species. Additionally, the protonation state of the benzoic acid group in fluorescein is known to have only a small effect on the location of its absorption maximum.[51,52] Thus we anticipate that calculations on **7** will produce a vertical excitation spectrum similar to that of **6** .

Gas-phase TD-B3LYP/SV(P) predicts for **7** an optically weak transition at 2.30 eV (oscillator strength $f < 0.01$). An attachment-detachment density plot indicates substantial CT character from the proton-free DPA arm to the xanthone ring (Figure 3). A second CT state, in which the proton-coordinating arm acts as the electron donor, is identified at 2.97 eV ($f = 0.03$). A bright excited state at 2.81 eV ($f = 0.33$) lies between the two CT states and is attributed to excitation within the conjugated π system of the xanthone ring. We judge the SV(P) basis to be sufficiently complete for our purposes by noting that low-lying excited state energies computed with the aug-cc-pVDZ basis set differ by less than 0.03 eV from their SV(P) counterparts.

We observe a moderate solvatochromic shift in the absorption spectrum of **7** in aqueous solution. The COSMO model predicts a blueshift of less than 0.05 eV for the bright state, while the low-lying CT state is stabilized by 0.1 eV due to its larger dipole moment. COSMO solvation removes CT contamination from the spectra of structures **4** through **6**; their energies and orbital character are summarized in Table 1. Structure **5** with its single protonated binding pocket exhibits a CT state 0.48 eV lower in energy than the lowest bright state, while the lowest valence and CT states

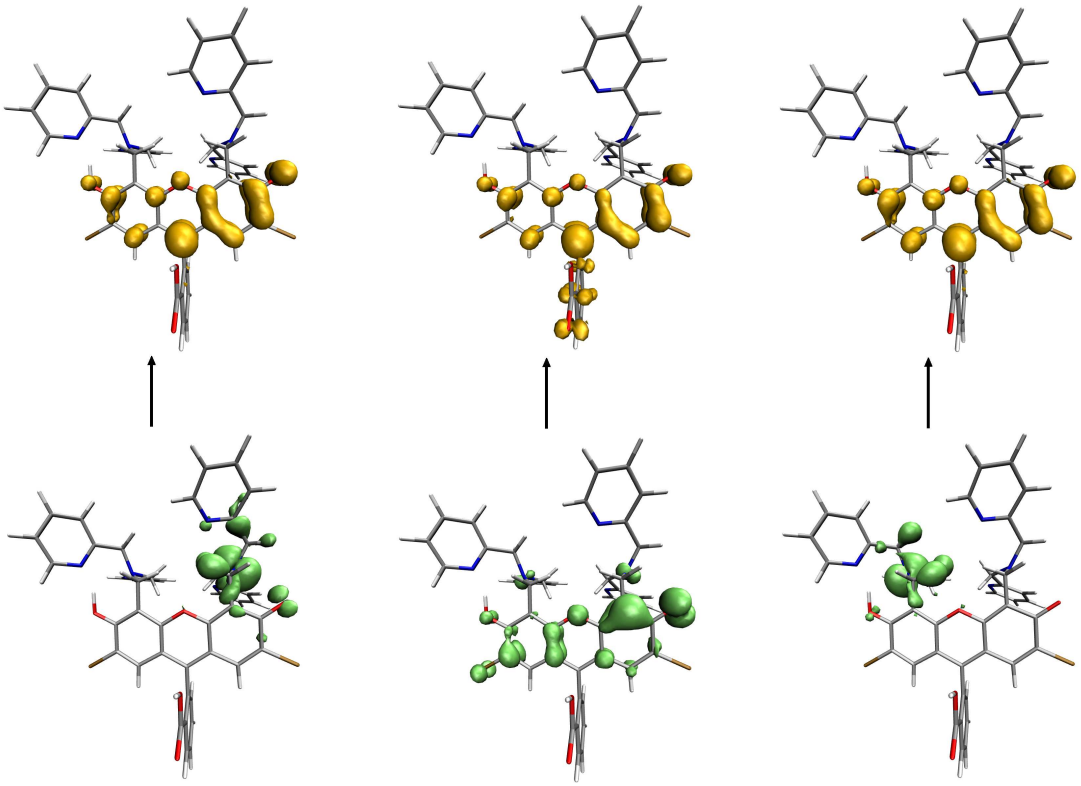

Figure 3: ZP1 attachment-detachment densities for low-lying excitations (from left to right): lowest CT, valence, and second-lowest CT excitation.[53]

of structures **4** and **6** are too close in energy for us to draw any conclusions about their relative ordering.

For structures **5** and **7**, which each have one protonated and one free binding pocket, the relative ordering of the CT and bright excited states supports the claim that fluorescence in metal-free ZP1 is quenched by ET to a lower-energy dark state, and the attachment-detachment densities suggest that it is reasonable to classify the PET process in this system qualitatively as electron donation from an amino nitrogen lone pair to the xanthone ring. Furthermore, in both **5** and **7**, the protonated arm's CT state is higher in energy than the bright state, which is consistent with the moderate fluorescence activation observed experimentally for conditions under which both binding pockets are protonated.

Table 1: TDDFT vertical excitation energies of the lowest valence and two lowest CT states of ZP1, evaluated with the B3LYP functional, SV(P) basis set, and COSMO solvation model. The lowest excitation energy for each structure is indicated in boldface.

Structure		Excitation energy (eV)			
Label	Zn^{2+}	expt.	valence	CT_1	CT_2
4	0		**2.86**	2.89	3.20
5	0	2.41	2.92	**2.44**	3.13
6	0		**3.02**	3.24	3.27
7	0		2.85	**2.21**	2.90
8	1		2.92	**2.84**	> 4.0
9	1		2.89	**2.33**	> 4.0
10	1		**2.92**	3.14	> 4.0
11	2	2.44	**2.84**	> 3.0	> 4.0

Next we consider changes to the vertical excitation spectrum of ZP1 upon binding one Zn^{2+} ion. We considered three protonation states for Zn-ZP1, corresponding to structures **8** through **10** in Figure 2. TD-B3LYP with COSMO solvation (Table 1) predicts that the CT state of structures **8** and **9**, which each retain an empty binding pocket, will lie lower in energy than the valence excited state, and thus continue to quench fluorescence. On the other hand, structure **10**, in which both binding pockets are occupied by an ion, exhibits a CT excited state at $\Delta E = 3.14$ eV, 0.22

eV above the valence excited state at $\Delta E = 2.92$ eV. This pattern corroborates the hypothesis that occupation of both binding sites by any coordinating ion is sufficient to alter the energy level ordering and activate the sensor's fluorescence.

TD-B3LYP places the bright state of Zn_2-ZP1 (structure **11**) at 2.84 eV, essentially unperturbed from that of metal-free ZP1. No CT states below 4.0 eV were identified in its vertical excitation spectrum, corroborating the claim that PET is unavailable for fluorescence quenching in Zn_2-ZP1.

The valence excitation energy predicted by TD-B3LYP with COSMO for the various ZP1 structures deviates substantially from the experimental absorption maximum at 2.41 eV. Our disagreement with experiment on the absorption maximum of ZP1 is concerning but not unprecedented; B3LYP has previously been reported to overestimate absolute valence excitation energies in some chromophores.[54,55] Whether this error in absolute excitation energies affects the relative ordering of the excited states is uncertain. The valence excited state energy is an overestimate while the CT excited state energies are probably underestimates. It remains conceivable that the valence state actually lies beneath the CT state in ZP1, so we turn to the alternative methods described below for further investigation.

TDDFT with long-range corrected functionals

While B3LYP results are in line with the proposed PET mechanism, they could be considered inconclusive for at least two reasons. First, we do not know whether overestimation of the valence excited state impacts the predicted ordering of the excited states. Second, as mentioned earlier, hybrid functionals in TDDFT are known to underestimate, sometimes severely, the energy of CT excited states. Methods which employ exact (nonlocal) exchange, such as configuration interaction singles (CIS),[56,57] should not suffer the latter pitfall. However, CIS greatly overestimates the excitation energy of the valence excited state (see the Supporting Information) and does not predict a lower-lying CT state in any of the ZP1 structures we studied. Therefore, we employed the long-

range corrected ωLRC-PBE and ωLRC-PBE0 functionals,[58] which pair the success of semilocal and hybrid functionals for local excited states with a correct description of exchange at long range.

The performance of these functionals has been previously benchmarked for excited states, with values for ω between 0.2 bohr^{-1} and 0.3 bohr^{-1} giving the least error in excitation energies for ωLRC-PBE and values in the vicinity of 0.1 bohr^{-1} performing best for ωLRC-PBE0; root-mean-square errors in these optimal parameter ranges are reported to be on the order of 0.3 eV.[39] However, ZP1 is significantly larger than any of the systems employed in the benchmarking study, so the previously determined values of ω may not be the most appropriate. We therefore decided to quantify the sensitivity of the excitation energies in ZP1 to the choice of ω.

A gas-phase LRC TDDFT calculation was carried out for metal-free ZP1 (structure **7**) and for Zn_2-ZP1 (structure **11**) at several reasonable[39] values of ω (Table 2). Here we find for neutral ZP1 that ωLRC-PBE places the CT state above the valence state for values of ω in the "optimal" range, but the CT state slides beneath the valence state for smaller values of ω. In contrast, our ωLRC-PBE0 calculations place the CT state beneath the valence state for the optimal choice of ω.

For the metal-free ZP1 anion **5**, ωLRC-PBE removes the spurious CT states as ω is increased. At $\omega = 0.1$ bohr^{-1}, there are at least six CT states beneath the lowest bright state, while the spectrum at $\omega = 0.3$ bohr^{-1} is entirely lacking in CT states beneath the bright state. The CT excitation energies are more strongly dependent on the choice of ω than the valence excitation energies because we are varying ω over distances that are beyond the characteristic length scale of the valence transition but are roughly commensurate with the CT transition. Still, both valence and CT excited states vary significantly as a function of ω.

These LRC functionals place the bright state of Zn_2-ZP1 below the first CT excited state, in agreement with TD-B3YLP and with the experimental observation of enhanced fluorescence in Zn_2-ZP1. Still, for metal-free ZP1 the optimal ωLRC-PBE functional places the valence state

Table 2: Lowest gas-phase valence and CT excitation energies of neutral ZP1 (in eV) predicted by long-range corrected PBE functionals, as a function of the range-separation parameter ω. The lowest excitation energy for each structure is indicated in boldface. Gas-phase TD-B3LYP/SV(P) predicts the lowest valence and CT states at 2.81 eV and 2.30 eV, respectively, for metal-free ZP1 and at 2.86 eV and $>$ 4.0 eV for Zn_2-ZP1.

ZP1	E_{ex}, ωLRC-PBE		E_{ex}, ωLRC-PBE0	
ω (a.u.)	valence	CT	valence	CT
0.10	2.63	**1.79**	2.96	**2.78**
0.15	2.72	**2.28**	**2.99**	3.18
0.20	2.89	**2.75**	**3.08**	3.48
0.25	**2.97**	3.20	**3.16**	3.70
0.30	**3.07**	3.47	**3.23**	3.86
Zn_2-ZP1				
ω (a.u.)	valence	CT	valence	CT
0.10	**2.68**	$>$ 4.0	**2.97**	$>$ 4.0
0.15	**2.81**	$>$ 4.0	**3.04**	$>$ 4.0
0.20	**2.92**	$>$ 4.0	**3.10**	$>$ 4.0
0.25	**3.01**	$>$ 4.0	**3.17**	$>$ 4.0
0.30	**3.10**	$>$ 4.0	**3.25**	$>$ 4.0

below the CT state, while the optimal ωLRC-PBE0 functional places the valence state above the CT state. Hence, it appears that these functionals are unable to clearly resolve the energy level ordering of the CT and bright states in metal-free ZP1.

With semilocal functionals, CT state contamination of the spectrum may actually play an important role in the cancellation of errors that makes certain TDDFT excitation energies so accurate. By lifting this contamination, long-range corrections can throw the error cancellation out of balance. The ωLRC-PBE valence excitation energies in metal-free ZP1 illustrate this trend, drifting increasingly further from the experimental value of 2.41 eV as ω is increased (Table 2). Given the LRC functionals' ambiguous excited state ordering for ZP1, we anticipate similar problems for the more challenging case of Zn-ZP1. Therefore, we turn to CDFT as an independent probe of the CT excited states.

CT excited states via CDFT

CDFT provides a wholly alternative route to the characterization of CT excited states in ZP1. We consider two definitions for the CDFT constraint regions. In one approach, one DPA arm is selected to be the donor region while the other arm comprises a spectator region with no applied constraint. In the other approach, both arms are assigned to the donor region. The DCF body of ZP1 defines the acceptor region in both cases. While the single-arm partitioning scheme is in keeping with our simple model of PET fluorescence quenching in this system, the two-arm scheme is desirable for its flexibility to permit some delocalization of the positive charge over both arms in the CT state.

Under the two-arm partitioning scheme, gas-phase CDFT with B3LYP predicts a CT state at 2.44 eV for structure **7**. Onsager solvation with the Pekar partitioning scheme stabilizes the CT state by 0.05 eV. A Becke population analysis of the constrained density (Figure 4a) indicates that the amine lone pair on the proton-free arm dominates the electron donation, while 31% of the donated density is attributed to the other arm. The population analysis also indicates a small contribution per pyridyl ring that cumulatively accounts for 32% of the transferred electron. These results corroborate the qualitative picture of PET in ZP1 as electron donation from the proton-free amine nitrogen to the xanthone ring; still, a quantitative understanding of the excited states requires us to consider the role of the pyridyl rings as partial electron donors.

If instead a single arm is constrained to serve as the electron donor, the predicted gas-phase CT state energy increases substantially. For example, the CT state of **7** was raised to 2.82 eV by constraining the arm near the phenolic oxygen (left side of the structure in Figure 2) to be the donor, while a CT excitation energy of 3.47 eV was found by treating the other arm as the donor.

The donor and acceptor regions of Zn-ZP1 and Zn_2-ZP1 are defined by analogy to the metal-free case, with zinc and any coordinated water assigned to the donor region. We found that this partitioning scheme led to unphysically large CT energy gaps ($\Delta E > 8$ eV) when a xanthone car-

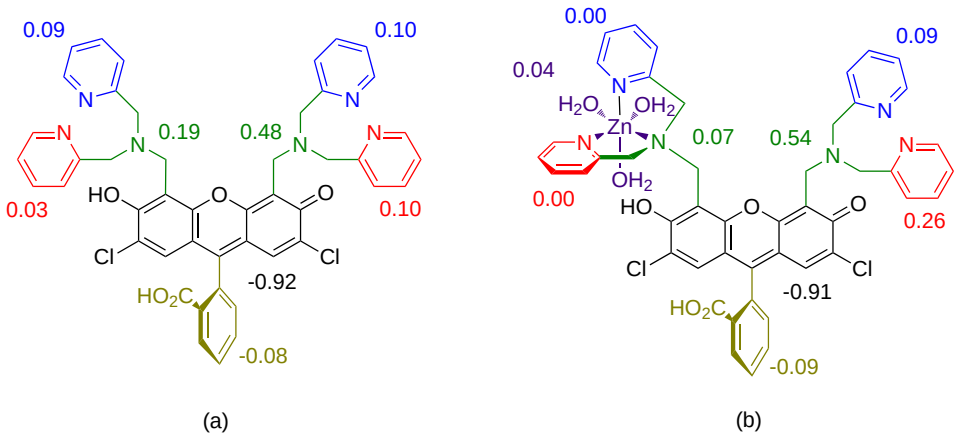

Figure 4: Net charge transfer by functional group upon excitation to the lowest CT state of ZP1 with (a) no zinc bound and (b) 1 zinc bound, computed using CDFT with B3LYP and Onsager solvation. The number of electrons is obtained from the Becke population on each highlighted group.

bonyl oxygen is covalently bonded to zinc, as in structure **2**. Therefore we choose to focus on structures in which zinc coordinates exclusively to the chelating nitrogens and water, in spite of crystallographic evidence that Zn binds preferentially to the carbonyl oxygen near the coordinating arm.[8] To test whether this structural alteration could severely change the excitation spectrum, we computed low-lying TD-B3LYP/SV(P)/COSMO excitation energies of the xanthone-chelating structure **2**, with the pocket proton shown in the figure removed. These energies were found to differ by less than 0.1 eV from their counterparts in the analogous structure **8**, suggesting that the additional separation of zinc from the xanthone ring will not drastically alter the ordering of the excited states.

CDFT/B3LYP with Onsager solvation places the CT state of Zn-ZP1 above the valence state regardless of whether the metal-free arm is protonated (Figure Table 3). A CT state at 3.59 eV is found if the phenolic proton is placed by the same arm as the bound Zn^{2+} (structure **9**), and this energy increases to 4.46 eV if the phenolic proton is moved to the Zn-free arm (structure **10**). Because the TDDFT bright state lies below 3 eV for each of these structures, fluorescence enhancement is possible with only one bound Zn^{2+} ion.

Population analysis of the CT state of Zn-ZP1 shows that the electron-donating region is more localized on a single arm than in the case of metal-free ZP1: for structure **9** (Figure 4b), 89% of the donated electron in Zn-ZP1 comes from one arm, compared with 68% for metal-free ZP1. The population analysis suggests that Zn^{2+} lifts the lowest CT state energy in part by reducing the coordinating arm's participation in electron donation.

For Zn_2-ZP1, the CT state is unambiguously inaccessible as a photophysical intermediate; CDFT/B3LYP with Onsager solvation places it 7.74 eV above the ground state. The high energy of this state can be rationalized from a molecular orbital perspective by noting that the CT excited state in Zn_2-ZP1 is produced by excitation from a Zn-N bonding orbital instead of a lone pair orbital.

Table 3: Valence excitation energies from TDDFT and CT excitation energies from CDFT, both in eV. See Figure 2 for structure details. All CDFT energies are at the B3LYP/SV(P) level with Onsager solvation.

Structure		Excitation energy (eV)	
Label	Zn^{2+}	valence (TDDFT)	CT (CDFT)
7	0	2.85	**2.39**
8	1	**2.90**	4.51
9	1	**2.89**	3.59
10	1	**2.92**	4.46
11	2	**2.84**	7.74

TDDFT and CDFT both place the lowest CT state of metal-free ZP1 beneath the bright state, and both predict a bright state beneath the lowest CT state for Zn_2-ZP1. For the more challenging case of Zn-ZP1, CDFT consistently predicts a bright state lying beneath the lowest CT state. TDDFT is at odds with this ordering for two of the three Zn-ZP1 structures we considered, but both methods show a marked increase in the CT state energy upon protonation of at least one binding pocket. These results suggest that PET fluorescence quenching in ZP1 can be deactivated by a single Zn^{2+} ion at physiological pH, where protonation of a binding pocket is common.

We caution that the limited separation of the donor and acceptor in this system makes CDFT energies sensitive to the way the atomic populations are defined and to the choice of donor-acceptor partition. One could examine whether this sensitivity is drastic enough to alter the predicted energy level ordering in ZP1 by varying the location of the partition, but there is little flexibility in the choice of partition for the well-defined donor-acceptor structure of ZP1.

We do not have a simple guideline for determining under what conditions CDFT will provide a more reasonable CT excitation energy than conventional or long-range corrected TDDFT. The two methods are more reliable in opposite limits; that is, TDDFT is well-suited to the description of localized excited states while CDFT performs best in the limit of long-range charge transfer excitations. Hence the two methods are in some sense complementary. Intramolecular CT in small PET sensors lies somewhere in the middle of these two extremes. While TDDFT is indispensable for the determination of valence excited states in molecules with tens to hundreds of atoms, we find that CDFT provides a competitive alternative for the study of intramolecular CT excited states.

Conclusion

We have carried out a two-pronged DFT study on the viability of the photoinduced electron transfer mechanism of fluorescence quenching in ZP1. An emphasis was placed on an accurate description of the charge transfer excited state believed to be responsible for quenching the fluorescence, which we characterized by TDDFT with hybrid and LRC functionals, and also by CDFT. TD-B3LYP predicts an energy level ordering consistent with the PET mechanism for zinc-free and zinc-saturated ZP1. TDDFT corroborates the experimentally motivated hypothesis that fluorescence is enhanced in ZP1 whenever both ion-binding sites are occupied. CDFT also places the CT excited states at energies consistent with PET fluorescence quenching in the zinc-free and zinc-saturated cases. Furthermore, CDFT and TDDFT both predict activation of the fluorescence upon binding of a single Zn^{2+} ion if the other binding pocket is protonated. CDFT enables population analysis on the CT excited state, which provides insight into the PET mechanism in ZP1 by

reporting that the donated electron density is largely localized on one arm's amine nitrogen.

This study illustrates the special challenge that intramolecular ET presents for CDFT, which can largely be traced to the definition of the donor and acceptor fragment densities. CDFT is naturally better suited for intermolecular CT because the partition between donor and acceptor densities in such cases is more clearly defined. For intramolecular CT, it is important to be aware of the increased sensitivity of the computed energy to the location of the partition and to the partitioning scheme in use. Furthermore, a non-integer charge constraint might be more appropriate than an integer constraint for molecules with limited donor-acceptor separation like ZP1. Several proposals for reducing the sensitivity of CDFT energies to these details are currently under investigation.

Looking forward, we would like to apply the methods described in this study to next-generation fluorescein-based sensors. In particular, we are interested in the evaluation and development of ratiometric sensors such as ZPP1, in which the fluorescence intensity of the sensor depends strongly on whether one or two Zn^{2+} ions are bound, enabling quantitation of zinc.[29]

It would also be useful to model the binding affinities of ZP1 and its derivatives for other transition metal ions. While experimental binding affinities are available for ZP1 with several transition metal ions, a computational approach would enable us to study metal ion affinities for a wide variety of ZP1 derivatives without having to synthesize each derivative.

Finally, it would be very desirable to have a method for predicting the degree of fluorescence activation conferred by the binding of a particular ion to ZP1. The fluorescence quantum yield of a molecule in dilute solution is a complicated function of the various decay pathways available to the molecule upon photoabsorption, and the rate constants of these processes are very sensitive to the molecular environment. We are not aware of any systematic approach in the literature for the *ab initio* computation of fluorescence quantum yields of luminescent molecules, but we believe that it would be an interesting and fruitful avenue to explore.

Acknowledgement

We thank Dr. Brian A. Wong and Prof. Stephen J. Lippard for experimental insights and useful discussions. We also thank Dr. Chiao-Lun Cheng for providing an implementation of fast-slow polarization separation in the Onsager SCRF method. TK acknowledges a Solar Revolution Project Fellowship from the Chesonis Family Foundation. TV acknowledges support from an NSF CAREER award (CHE-0547877) and fellowships from the Packard Foundation and the Sloan Foundation.

Supporting Information Available

Optimized B3LYP/SV(P)/COSMO geometries for each ZP1 structure in Figure 2, and associated TDDFT, CIS and CDFT excitation energies. This material is available free of charge via the Internet at `http://pubs.acs.org/`.

References

(1) *Photoinduced Electron Transfer*; Fox, M. A., Chanon, M., Eds.; Elsevier, 1988.

(2) Davidson, R. S. *Advances in Physical Organic Chemistry* **1983**, *19*, 1–130.

(3) Lakowicz, J. R. *Principles of Fluorescence Spectroscopy*; Springer, 2006.

(4) Callan, J. F.; de Silva, A. P.; Magri, D. C. *Tetrahedron* **2005**, *61*, 8551–8588.

(5) de Silva, A. P.; Gunaratne, H. Q.; Gunnlaugsson, T.; Huxley, A. J.; McCoy, C. P.; Rademacher, J. T.; Rice, T. E. *Chem. Rev.* **1997**, *97*, 1515–1566.

(6) Nolan, E. M.; Lippard, S. J. *Acc. Chem. Res.* **2009**, *42*, 193–203.

(7) Walkup, G. K.; Burdette, S. C.; Lippard, S. J.; Tsien, R. Y. *J. Amer. Chem. Soc.* **2000**, *122*, 5644–5645.

(8) Wong, B. A.; Friedle, S.; Lippard, S. J. *J. Amer. Chem. Soc.* **2009**, *131*, 7142–7152.

(9) Rurack, K. *Spectrochim. Acta A* **2001**, *57*, 2161–2195.

(10) Serranoandres, L.; Merchan, M.; Roos, B.; Lindh, R. *J. Amer. Chem. Soc.* **1995**, *117*, 3189–3204.

(11) Jin, T.; Ichikawa, K.; Koyama, T. *J. Chem. Soc., Chem. Commun.* **1992**, 499–501.

(12) Clapp, A. R.; Medintz, I. L.; Mattoussi, H. *ChemPhysChem* **2006**, *7*, 47–57.

(13) Cukier, R. I.; Nocera, D. G. *Ann. Rev. Phys. Chem.* **1998**, *49*, 337–369.

(14) Prashanthi, S.; Bangal, P. R. *Chem. Comm.* **2009**, 1757–1759.

(15) Bhattacharya, S.; Pradhan, T. K.; De, A.; Chaudhury, S. R.; De, A. K.; Ganguly, T. *J. Phys. Chem. A* **2006**, *110*, 5665–5673.

(16) Han, F.; Chi, L.; Liang, X.; Ji, S.; Liu, S.; Zhou, F.; Wu, Y.; Han, K.; Zhao, J.; James, T. D. *J. Org. Chem.* **2009**, *74*, 1333–1336.

(17) Lim, M. H.; Wong, B. A.; Pitcock, W. H., Jr.; Mokshagundam, D.; Baik, M.-H.; Lippard, S. J. *J. Amer. Chem. Soc.* **2006**, *128*, 14364–14373.

(18) Petsalakis, I. D.; Lathiotakis, N. N.; Theodorakopoulos, G. *J. Mol. Struct. Theochem.* **2008**, *867*, 64–70.

(19) Petsalakis, I. D.; Kerkines, I. S. K.; Lathiotakis, N. N.; Theodorakopoulos, G. *Chem. Phys. Lett.* **2009**, *474*, 278–284.

(20) McCarroll, M. E.; Shi, Y.; Harris, S.; Puli, S.; Kimaru, I.; Xu, R.; Wang, L.; Dyer, D. *J. Phys. Chem. B* **2006**, *110*, 22991–22994.

(21) Dreuw, A.; Weisman, J. L.; Head-Gordon, M. *J. Chem. Phys.* **2003**, *119*, 2943–2946.

(22) Wu, Q.; Van Voorhis, T. *Phys. Rev. A* **2005**, *72*, 024502.

(23) Wu, Q.; Van Voorhis, T. *J. Chem. Theory Comput.* **2006**, *2*, 765–774.

(24) Wong, B. A.; Friedle, S.; Lippard, S. J. *Inorg. Chem.* **2009**, *48*, 7009–7011.

(25) Sparano, B. A.; Shahi, S. P.; Koide, K. *Org. Lett.* **2004**, *6*, 1947–1949.

(26) Burdette, S. C.; Frederickson, C. J.; Bu, W.; Lippard, S. J. *J. Amer. Chem. Soc.* **2003**, *125*, 1778–1787.

(27) Nolan, E. M.; Lippard, S. J. *Inorg. Chem* **2004**, *43*, 8310–8317.

(28) Nolan, E. M.; Jaworski, J.; Okamoto, K. I.; Hayashi, Y.; Sheng, M.; Lippard, S. J. *J. Amer. Chem. Soc.* **2005**, *127*, 16812–16823.

(29) Zhang, X.; Hayes, D.; Smith, S. J.; Friedle, S.; Lippard, S. J. *J. Amer. Chem. Soc.* **2008**, *130*, 15788–15789.

(30) Woodroofe, C. C.; Masalha, R.; Barnes, K. R.; Frederickson, C. J.; Lippard, S. J. *Chem. Biol.* **2004**, *11*, 1659–1666.

(31) Malavolta, M.; Costarelli, L.; Giacconi, R.; Muti, E.; Bernardini, G.; Tesei, S.; Cipriano, C.; Mocchegiani, E. *Cytom. Part A* **2006**, *69A*, 1043–1053.

(32) Anderegg, G.; Hubmann, E.; Podder, E.; Wenk, N. G. *Helv. Chim. Acta* **1977**, *60*, 123–140.

(33) Becke, A. D. *J. Chem. Phys.* **1993**, *98*, 5648–5652.

(34) Lee, C. T.; Yang, W. T.; Parr, R. G. *Phys. Rev. B* **1988**, *37*, 785–789.

(35) Ahlrichs, R.; Bar, M.; Haser, M.; Horn, H.; Kolmel, C. *Chem. Phys. Lett.* **1989**, *162*, 165–169.

(36) Weigend, F.; Ahlrichs, R. *Phys. Chem. Chem. Phys.* **2005**, *7*, 3297–3305.

(37) Figgen, D.; Rauhut, G.; Dolg, M.; Stoll, H. *Chem. Phys.* **2005**, *311*, 227–244.

(38) Klamt, A.; Schüürmann, G. *J. Chem. Soc., Perkin Trans. 2* **1993**, 799–805.

(39) Rohrdanz, M. A.; Martins, K. M.; Herbert, J. M. *J. Chem. Phys.* **2009**, *130*, 054112.

(40) Shao, Y. et al. *Phys. Chem. Chem. Phys.* **2006**, *8*, 3172–3191.

(41) Head-Gordon, M.; Graña, A. M.; Maurice, D.; White, C. A. *J. Phys. Chem.* **1995**, *99*, 14261–14270.

(42) Hirata, S.; Head-Gordon, M. *Chem. Phys. Lett.* **1999**, *314*, 291–299.

(43) Dunning, Jr., T. H. *J. Chem. Phys.* **1989**, *90*, 1007.

(44) Becke, A. D. *J. Chem. Phys.* **1988**, *88*, 2547–2553.

(45) Bayliss, N. S.; McRae, E. G. *J. Phys. Chem.* **1954**, *58*, 1002–1006.

(46) Cramer, C. J.; Truhlar, D. G. *Chem. Rev.* **1999**, *99*, 2161–2200.

(47) Onsager, L. *J. Amer. Chem. Soc.* **1936**, *58*, 1486–1493.

(48) Foresman, J. B.; Keith, T. A.; Wiberg, K. B.; Snoonian, J.; Frisch, M. J. *J. Phys. Chem.* **1996**, *100*, 16098–16104.

(49) Aguilar, M. A. *J. Phys. Chem. A* **2001**, *105*, 10393–10396.

(50) Zhang, X.-F.; Liu, Q.; Son, A.; Zhang, Q.; Zhao, F.; Zhang, F. *J. Fluoresc.* **2008**, *18*, 1051–1057.

(51) Sjoback, R.; Nygren, J.; Kubista, M. *Spectrochim. Acta* **1995**, *51*, L7–L21.

(52) Casanovas, J.; Jacquemin, D.; Perpète, E. A.; Alemán, C. *Chem. Phys.* **2008**, *354*, 155–161.

(53) Humphrey, W.; Dalke, A.; Schulten, K. *J. Mol. Graphics* **1996**, *14*, 33–38.

(54) Wanko, M.; Garavelli, M.; Bernardi, F.; Niehaus, T. A.; Frauenheim, T.; Elstner, M. *J. Chem. Phys.* **2004**, *120*, 1674–1692.

(55) Wiberg, K. B.; Stratmann, R. E.; Frisch, M. J. *Chem. Phys. Lett.* **1998**, *297*, 60–64.

(56) Del Bene, J. E.; Ditchfield, R.; Pople, J. A. *J. Chem. Phys.* **1971**, *55*, 2236–2241.

(57) Foresman, J. B.; Head-Gordon, M.; Pople, J. A.; Frisch, M. J. *J. Phys. Chem.* **1992**, *96*, 135–149.

(58) Rohrdanz, M. A.; Herbert, J. M. *J. Chem. Phys.* **2008**, *129*, 034107.

Graphical TOC Entry